Hindawi Publishing Corporation
International Journal of Photoenergy
Volume 2014, Article ID 793723, 7 pages
http://dx.doi.org/10.1155/2014/793723

Hindawi

Research Article

Photophysical Properties of Pheophorbide-a Derivatives and Their Photodynamic Therapeutic Effects on a Tumor Cell Line *In Vitro*

Kang-Kyun Wang,[1] Jing Li,[1] Bong-Jin Kim,[1] Jeong-Hyun Lee,[1] Hee-Won Shin,[1] Si-Hwan Ko,[2] Won-Young Lee,[2] Chang-Hee Lee,[3] Seok Hoon Jung,[4] and Yong-Rok Kim[1]

[1] *Department of Chemistry, Yonsei University, 50 Yonsero, Seodaemun-Gu, Seoul 120-749, Republic of Korea*
[2] *Department of Microbiology, College of Medicine, Yonsei University, Seoul 120-752, Republic of Korea*
[3] *Department of Chemistry, Kangwon National University, Chuncheon 200-701, Republic of Korea*
[4] *Department of Laboratory Medicine and Research Institute of Bacterial Resistance, College of Medicine, Yonsei University, 211 Eonjuro, Gangnam-Gu, Seoul 135-720, Republic of Korea*

Correspondence should be addressed to Seok Hoon Jung; kscpjsh@yuhs.ac and Yong-Rok Kim; yrkim@yonsei.ac.kr

Received 20 May 2014; Revised 24 July 2014; Accepted 24 July 2014; Published 10 August 2014

Academic Editor: Leonardo Palmisano

Pheophorbide-a derivatives have been reported to be potential photosensitizers for photodynamic therapy (PDT). In this study, photophysics of pheophorbide-a derivatives (PaDs) were investigated along with their photodynamic tumoricidal effect *in vitro*. PaDs were modified by changing the coil length and/or making the hydroxyl group (–OH) substitutions. Their photophysical properties were studied by steady-state and time-resolved spectroscopic methods. The photodynamic tumoricidal effect was evaluated in the mouse breast cancer cell line (EMT6). Lifetime and quantum yield of fluorescence and quantum yields of triplet state and singlet oxygen were studied to determine the dynamic energy flow. The coil length of the substituted alkyl group did not significantly affect the spectroscopic properties. However, the substitution with the hydroxyl group increased the quantum yields of the triplet state and the singlet oxygen due to the enhanced intersystem crossing. In order to check the application possibility as a photodynamic therapy agent, the PaDs with hydroxyl group were studied for the cellular affinity and the photodynamic tumoricidal effect of EMT6. The results showed that the cellular affinity and the photodynamic tumoricidal effect of PaDs with the hydroxyl group depended on the coil-length of the substituted alkyl group.

1. Introduction

Photodynamic therapy (PDT), a minimally invasive treatment method for a multitude of diseases including cancer, uses reactive oxygen species (ROS) that are generated from photoexcited photosensitizers [1]. After the cancer cells localize the photosensitizer, this photodynamic compound absorbs an appropriate wavelength of light and generates ROS through both energy and charge transfer processes [2]. Among the generated ROS, singlet oxygen is one of the important species that have the high oxidation capacity that damages the cancer cells [3]. The singlet oxygen can be produced through the energy transfer process from the triplet state of the photosensitizer to the triplet oxygen molecules [2]. Therefore, the triplet state quantum yield of a photosensitizer is one of the major factors influencing singlet oxygen generation [4]. There are number of desirable photophysical properties for the photosensitizer agent of PDT application. Not only does the photosensitizer need to have a good cellular affinity [5, 6], but also it should possess the high singlet oxygen generation efficiency [7]. In addition, since the red light penetrates the tissue more deeply with a minimal light loss in biological media [8], the photosensitizer that absorbs the red light is also preferred.

In that aspect, pheophorbide-a derivatives (PaDs), hematoporphyrin derivatives (HpDs), and indocyanine green (ICG) are considered to be the efficient photosensitizers for the diagnosis and the treatment of tumors [8, 9]. Previous studies suggest that PaDs are potentially valuable photosensitizers due to their favored optical properties that include the long wavelength absorption and the high singlet oxygen quantum yields, compared with HpDs and ICG [10–12].

In this study, we investigated the photophysical properties of pheophorbide-a derivatives (PaDs) and their photodynamic biological activities *in vitro*. In particular, the photophysical factors influencing singlet oxygen generation were studied in terms of the substitution effect of the hydroxyl groups and the coil length difference of the alkyl groups of PaDs. Also, for the possibility of PDT application, cellular affinity and photodynamic tumoricidal effect of PaDs were investigated with mouse breast cancer cell line (EMT6) *in vitro*.

2. Materials and Methods

2.1. Materials. Pheophytin-a (PA) and 10-hydroxylpheophytin-a (HPA) were extracted from silkworm excreta. Other PaDs including pheophorbide-a propyl ester (PPE), 10-hydroxylpheophorbide-a propyl ester (HPPE) pheophorbide-a methyl ester (PME), and 10-hydroxylpheophorbide-a methyl ester (HPME) were synthesized and characterized as previously reported [13–16]. As shown in Figure 1, PA, PPE, and PME were modified by changing the coil length of the substituted alkyl group (PaD-alkyls), and HPA, HPPE, and HPME were modified with the substitution of the hydroxyl group (PaD-OHs). Toluene (Merck, HPLC grade) was used as a solvent for all samples without further purification. Degassed toluene was prepared by ten times of freeze-thaw-pump cycle. Air-saturated toluene was prepared by bubbling air gas for 40 minutes. Concentration of the samples was controlled to be in the range of 10^{-5} M.

2.2. Spectroscopy Measurements. Steady-state absorption and emission spectra were obtained using a UV-Vis spectrophotometer (Shimadzu, UV-160A) and a spectrofluorimeter (Hitachi, F-4500), respectively. A N_2 laser-pumped dye laser (Laser Photonics, LN1000, 600 ps FWHM pulse) was used as an excitation source for time-resolved fluorescence. Fluorescence from the samples was collected perpendicular to the excitation beam and detected with a monochromator (Acton Research, SpectraPro) and photomultiplier tube (PMT, Hamamatsu, H5783-04) at the magic angle. The signals were processed by a 500 MHz digital oscilloscope (Hewlett Packard, 54520A) and transferred to a computer for data analysis [17]. Time-resolved triplet-triplet absorption spectra were measured by using a xenon lamp as a probe source. The probe light from the xenon lamp was shaped by an iris and then perpendicularly focused on the sample that was excited by the pump beam from Nd-YAG (BMI series, 7 ns FWHM pulse) pumped optical parametric oscillator (OPO) laser (BMI OP901-355, 5 ns FWHM pulse). The transmitted probe light was collected by focusing optics and then detected with a monochromator (Jobin Yvon, H20) and a PMT (Hamamatsu, R-928). The signals were processed by a 500 MHz digital oscilloscope (Hewlett Packard, 54520A) and then transferred to a computer [18, 19]. Triplet quantum yield was determined with various excitation powers by the power-dependent comparative method [18, 19].

The Nd-YAG-pumped OPO laser was utilized as an excitation source for the detection of time-resolved singlet oxygen phosphorescence. The phosphorescence signal was collected perpendicular to the excitation beam and detected with a germanium photodiode (EG&G, Judson). An interference bandpass (1270 nm, spectrogon) and cut-off filters (<1000 nm, CVI) were inserted between the sample and the detector window to remove the stray scattering light of laser excitation and the sample fluorescence that interfered with the phosphorescence signal. The signal was acquired by a 500 MHz digital oscilloscope and transferred to a computer. The singlet oxygen quantum yield was directly determined from the intensity of the singlet oxygen phosphorescence signal [19].

2.3. Biological Assay. For evaluation of cell uptake efficiency of photosensitizer, mean fluorescence intensity (MFI) of photosensitizer which was loaded to the cell was measured [20]. The EMT6 cells (1×10^6 in a 35 mm tissue culture dish) were incubated with 1.5 mL of DMEM with photosensitizers (0.1 μg/mL) for 1 hour at 37°C. These experiments were performed at the concentration range of PaDs where the nontoxicity was confirmed from previous reports [21, 22]. After incubation with photosensitizers, the cells were harvested from 35 mm tissue culture dish. The cells were washed twice with fresh phosphate buffered saline (PBS). Flow cytometry measurement was then performed using a fluorescence-activated cell sorting (FACS) flow cytometer (Becton Dickinson, Canto II) equipped with a single 488 nm argon laser. A minimum of 10,000 cells per sample was acquired in list mode and analyzed using LYSYS II software.

For the photodynamic tumoricidal activity assay *in vitro*, the photosensitizers were dissolved in pure N, N-dimethyl formamide (DMF) for the stock solution (10 μg/mL) and the stock solution was stored in the dark at −20°C. A light source of irradiation was a 200 W halogen lamp (MVI Micro Video Instruments Inc., MA, USA) with a 515 nm cut-off filter. Total power output of the irradiation was measured using a laser power meter (Metrologic Instruments, Inc., Blackwood, NJ, USA). The irradiation energy was controlled to be 1.2 J/cm^2. The mouse breast cancer cell line (EMT6 cells, 1×10^6 in a 35 mm tissue culture dish) was incubated with 1.5 mL of Dulbecco's modified Eagle's medium (DMEM) and the photosensitizers (0.1 μg/mL) for 1 hour at 37°C in dark condition. After incubation, the cells were exposed to light for PDT. Then, the cells were further incubated at 37°C for 24 hours in a dark humidified incubator [21]. After the incubation, the cells were harvested from the 35 mm tissue culture dish and 100 μL of MTT solution (1 mg/mL) was added to the cell pellets. The sample was incubated at 37°C in a dark humidified incubator. After 4 hours, the cells were centrifuged and the supernatant was discarded,

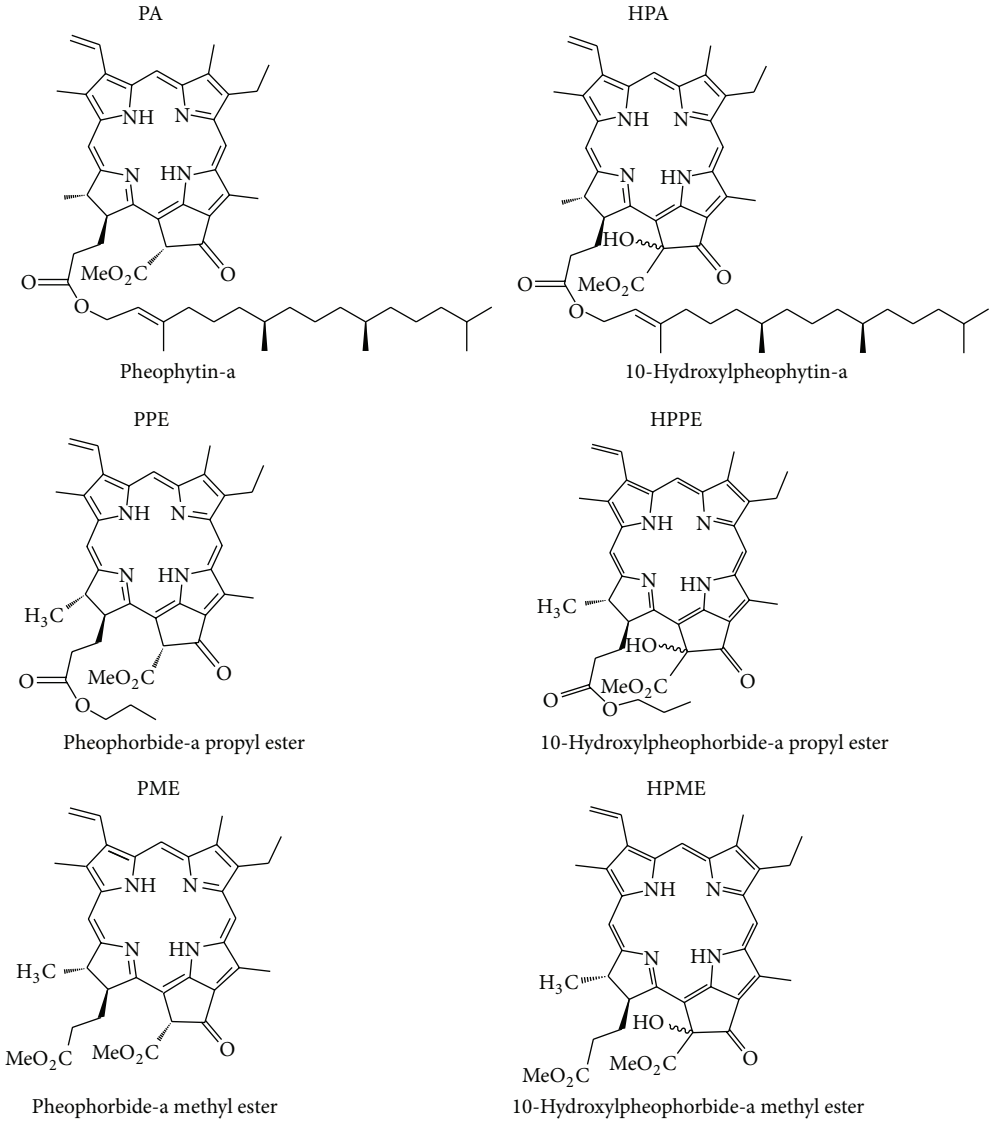

Figure 1: Molecular structures of pheophorbide-a derivatives (PaDs).

and the sample was washed with PBS. 100 μL of dimethyl sulfoxide (DMSO) was added to the sample for cell lysis. The reaction was stopped by the addition of 100 μL of isopropanol. The solution (100 μL) was loaded into 96-well microtiter plates. The absorbance was measured with an automated spectrophotometric microtiter plate reader (Spectra Max 340/Molecular Devices, USA) using a 570 nm filter [23].

3. Results and Discussion

The steady-state absorption and fluorescence spectra of PaDs are presented in Figure 2. The coil length of the substituted alkyl group in PaD-alkyls (PA, PPE, and PME) did not significantly affect the absorption spectra (not shown in the Figure). However, PaD-OHs (HPA, HPPE, and HPME) show slightly different spectral characteristics. The two peaks at 506 nm and 537 nm correspond to the Q_x transitions and the other two peaks at 610 nm and 667 nm are responsible for the Q_y transitions. The Q_x bands of PaD-OHs are shifted to the shorter wavelengths more than those of PaD-alkyls as shown in Figure 2(a), while the Q_y bands of PaD-OHs are consistent with those of PaD-alkyls [24–26]. It implies that the symmetric degeneracy of PaDs is influenced by hydroxyl group in the x-direction. The fluorescence spectra in Figure 2(b) presents the peaks at 677 and 725 nm and peaks are slightly red shifted due to the structural deformation by the substituted hydroxyl group.

The peak position of fluorescence maximum and the fluorescence quantum yields are listed in Table 1. The fluorescence quantum yields were independent of the concentration and the excitation wavelength, and the aggregation effect was not observed. The fluorescence spectra of all PaDs were similar to each other (data not shown). The fluorescence quantum yields were measured by a comparative method using

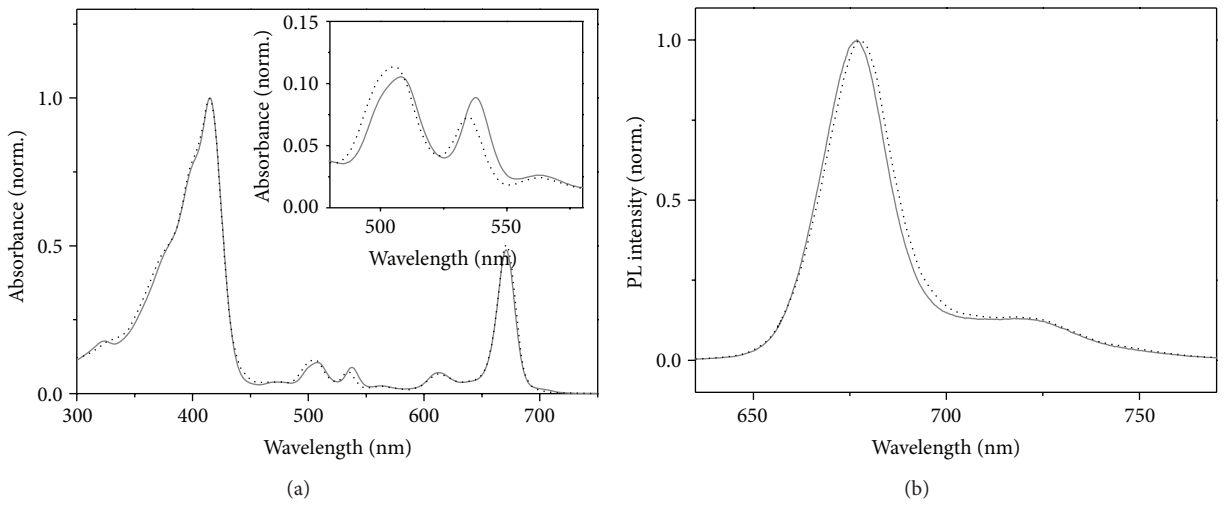

FIGURE 2: (a) Steady-state absorption spectra of PaDs. The details of Q_x-bands are shown in the inset. (b) Steady-state fluorescence (λ_{ex} = 507 nm) spectra of PaDs in toluene solution; PA (solid grey line) and HPA (dotted black line).

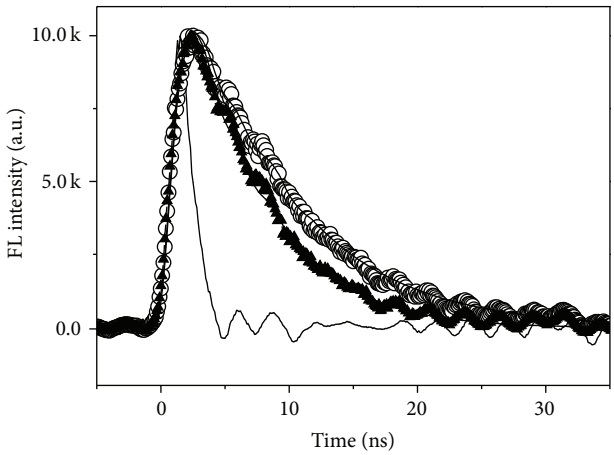

FIGURE 3: Typical fluorescence decay signals (λ_{ex} = 507 nm) and the fitted lines of PA (o) and HPA (▲); IRF indicates the instrumental response function (solid thin line).

a standard reference with the reported value (Φ_f of H_2TPP = 0.09 in toluene) as follows [19]:

$$\Phi_S = \Phi_R \left(\frac{A_R}{A_s}\right)\left(\frac{I(\lambda_R)}{I(\lambda_s)}\right)\left(\frac{n_s^2}{n_R^2}\right)\left(\frac{D_s}{D_R}\right). \quad (1)$$

In (1), the subscripts of s and R represent sample and reference, respectively, while n is the refractive index of the solution. I is the intensity of the excitation source at the given wavelength. A and D are the absorbance and the integrated fluorescence area, respectively [27]. The fluorescence quantum yield was reduced when the hydroxyl groups were added. However, the coil length of the substituted alkyl group in PaD-alkyls and PaD-OHs did not influence the fluorescence quantum yield.

Time-resolved fluorescence decay was measured at the peak position of emission band with the excitation wavelength of 507 nm (Figure 3). Fluorescence decay signals were well fitted to a single exponential with an iterative nonlinear deconvolution fitting method. The fluorescence decay rate did not show the detection wavelength dependence for all samples, implying that the emission state was homogeneity [28]. The fluorescence lifetime and the quantum yield of PaD-OHs were faster and smaller than those of PaD-alkyls as shown in Table 1. The fluorescence decay rate was determined using the following relationship:

$$k_f = k_r + k_{ic} + k_{isc}. \quad (2)$$

k_r, k_{ic}, and k_{isc} are radiative, internal conversion, and intersystem crossing rates of S_1 state, respectively, and they can be estimated as follows:

$$k_r = \Phi_f k_f, \qquad k_{isc} = \Phi_T k_f, \qquad k_{ic} = \left(1 - \Phi_f - \Phi_T\right) k_f. \quad (3)$$

The distortion in the π-conjugated macrocycle ring resulted in low fluorescence quantum yield due to the high intersystem crossing rates. And, therefore, the fluorescence lifetime became fastened.

The triplet state quantum yield was determined by the power dependent comparative method [25]:

$$\Delta\text{O.D.} = a\left(1 - \exp\left(-b \cdot E\right)\right). \quad (4)$$

In (4), a is a proportionality constant and b equals $k\Phi_T\varepsilon_g$ (Φ_T is a triplet quantum yield, ε_g is an absorption coefficient of the transition, and k is an instrumental constant). With the absorption coefficient of the ground state and the b values for both reference and sample, the triplet state quantum yields of PaDs are estimated as follows [27]:

$$\Phi_T^S = \Phi_T^R \frac{b^S \cdot \varepsilon_g^s}{b^R \cdot \varepsilon_g^s}. \quad (5)$$

Table 1: Photophysical parameters of the singlet excited state in degassed and air-saturated conditions.

Compound	$\lambda_{f,\max}$ (nm)	$\tau_f{}'$ (ns)	$\tau_f{}''$ (ns)	Φ_f	$k_f{}'$ (10^6 s^{-1})	$k_r{}'$ (10^6 s^{-1})	$k_{ic}{}'$ (10^6 s^{-1})	$k_{isc}{}'$ (10^6 s^{-1})
PA	677	9.0	7.9	0.26	111	33	4.4	77
PPE	677	9.2	7.8	0.26	109	33	3.2	77
PME	677	9.3	7.8	0.25	107	32	1.1	79
HPA	678	6.2	5.4	0.19	162	35	3.2	127
HPPE	678	6.7	5.8	0.18	149	31	3.0	119
HPME	678	6.4	5.6	0.20	156	37	1.5	123

Prime ($'$) and double prime ($''$) stand for degassed and air-saturated conditions, respectively.

Table 2: Summary of the parameter relative to the singlet oxygen quantum yield.

Compound	Φ_T	Φ_Δ	τ_Δ/μs	S_Δ^T	$P_{O_2}^T$
PA	0.69	0.62	29	0.84	~1
PPE	0.70	0.66	29	0.87	~1
PME	0.74	0.62	29	0.79	~1
HPA	0.79	0.71	29	0.87	~1
HPPE	0.80	0.73	29	0.89	~1
HPME	0.79	0.70	29	0.81	~1

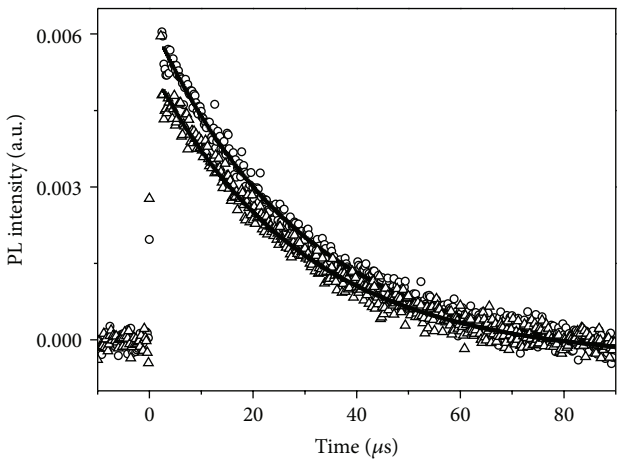

Figure 4: Time-resolved $^1O_2$ phosphorescence signals (λ_{ex} = 507 nm) and the fitted lines of PA (o) and HPA (△) in toluene solutions.

In (5), S and R represent the sample and the reference, respectively. Triplet state quantum yields (Φ_T^S) of PaDs were estimated using the H_2TPP reference value ($\Phi_T^R = 0.72$) in toluene solution (listed in Table 2) [29]. Estimated triplet state quantum yields of PaD-OHs were higher than those of PaD-alkyls. The enhanced triplet state quantum yield of the hydroxyl-substituted PaDs is due to the increased intersystem crossing rate as mentioned above.

Singlet oxygen phosphorescence was measured at the detection wavelength of 1270 nm under air-saturated condition. As shown in Figure 4, the singlet oxygen lifetime was estimated to be 29 μs in toluene. It correlates with the reported values of 27~29 μs [29]. Singlet oxygen quantum yields (Φ_Δ) were obtained using the following equation with the reference value of H_2TPP ($\Phi_\Delta = 0.68$) [29]:

$$\Phi_\Delta^S = \Phi_\Delta^R \frac{I_S \times \left(1 - 10^{-A_R}\right)}{I_R \times \left(1 - 10^{-A_S}\right)}. \quad (6)$$

I is the phosphorescence signal at time zero and A is the absorbance at the excitation wavelength. The indexes S and R correspond to the sample and the reference, respectively. The singlet oxygen quantum yields and lifetimes are shown in Table 2. The singlet oxygen quantum yields of PaD-OHs were higher than those of PaD-alkyls. The photophysical factors governing the relationship between the triplet state and the singlet oxygen were determined using the following expression [29]:

$$\Phi_\Delta^S = \Phi_T \cdot P_{O_2}^T \cdot S_\Delta^T, \quad (7)$$

$$P_{O_2}^T = \frac{k_q^T [O_2]^a}{k_T^0 + k_q^T [O_2]^a}, \quad (8)$$

$$k_T^a = k_T^0 + k_q^T [O_2]^a, \quad (9)$$

where Φ_T is the triplet quantum yield of the sample in degassed condition, $P_{O_2}^T$ is the fraction of the triplet states quenched by oxygen, and S_Δ^T is the efficiency of singlet oxygen generation induced by the energy transfer during the oxygen quenching of the triplet state. k_q^T is the oxygen quenching rate constant of the triplet state and a and d are the air-saturated and degassed conditions, respectively. The oxygen concentration of the air-saturated solution ($[O_2]^a$) of toluene at room temperature was estimated to be 2.1×10^{-3} M as in [29]. k_T^a was determined using the measured lifetime of the triplet state in the air-saturated condition. Since the intrinsic decay rate constant of the triplet state (k_T^0) for toluene was reported to be 1.0×10^3 s^{-1} in the literature [29], the oxygen quenching rate constant of the triplet state (k_q^T) was determined to be 1.6×10^9 s^{-1} from (9). Therefore, $P_{O_2}^T$ with the estimated values of k_q^T, k_T^0, $[O_2]^a$, and (8) resulted in the value of ~1. Therefore, the enhanced singlet oxygen quantum yields of the substituted hydroxyl groups are originated to increased intersystem crossing rate and the triplet state quantum yield [30, 31].

Table 3: Cellular affinity (MFI) and photodynamic tumoricidal effect (MTT) of PaD-OHs.

Compound	Φ_Δ	MFI	MTT
HPA	0.71	6.10	9.8
HPPE	0.73	29.05	24.1
HPME	0.70	66.51	76.7

To demonstrate the efficacy of PaDs for the application of the photodynamic therapy agent, PaD-OHs (HPA, HPPE, and HPME) that have higher singlet oxygen quantum yield than PaD-alkyls (PA, PPE, PME) were studied for the cellular affinity and the photodynamic inactivation with mouse breast cancer cells. The cells were treated with PaD-OHs (0.1 μg/mL) for one hour of uptake time. The mean fluorescent intensity (MFI) expressed by the cells was examined to determine the cellular affinity of photosensitizers [20]. The shorter coil length of the substituted alkyl group in PaD-OHs significantly enhanced cellular uptake efficiency of pheophorbide-a as shown in Table 3. The similar results were also reported in Rancan et al.'s work [32]. They suggested that, in the substitution group of photosensitizers, more polar groups with less alkyl chains showed more uptake efficiency. As the plausible explanation for this uptake efficiency, the less aggregation of photosensitizers and more efficient penetration through the membranes with the photosensitizer of high polarity were considered. Our results agreed with their work along with the same explanation. Photodynamic tumoricidal effect *in vitro* was determined using the 3-(4, 5-dimethylthiazol-2yl)-2, 5-diphenyl-2H-tetrazolium bromide (MTT) assay method. As shown in Table 3, HPME that has the short alkyl chain shows higher tumoricidal effect than HPA and HPPE do as expected.

4. Conclusion

The wavelength-shift in the absorption and emission spectra of PaD-OHs is due to the structural deformation of the π-conjugated macrocycle ring. Such structural deformation of PaD-OHs results in larger k_{isc} values and the reduced fluorescence quantum yield compared with PaD-alkyls. Therefore, it appears that the hydroxyl group substitution in the ring V of pheophorbide-a affects the electronic states of the π-conjugated macrocycle ring. However, the nonplanarity does not significantly change the k_{ic} values that are not sufficiently enough to enhance the nonradiative decay. The reduced fluorescence quantum yields and the fast lifetime are due to the enhanced intersystem crossing rate. On the other hand, the coil length of the substituted alkyl group does not significantly influence the spectroscopic properties of PaDs, suggesting that the coil length of PaDs does not influence the energy states of the photosensitizer.

The results on the cellular affinity and the photodynamic tumoricidal effect indicate that they are affected by the coil-length of the substituted alkyl group in PaD-OHs. It concludes that the hydroxyl substitution group improves the photophysical efficiencies of the photosensitizers and the shorter coil-length of the substituted alkyl group enhances the cellular affinity, and these are the photodynamic tumoricidal effects.

Conflict of Interests

The authors declare that there is no conflict of interests regarding the publication of this paper.

Acknowledgment

This work was supported by a grant of the Korea Healthcare Technology R&D Project, Ministry of Health & Welfare, Republic of Korea (A121133).

References

[1] K. Kalka, H. Merk, and H. Mukhtar, "Photodynamic therapy in dermatology," *Journal of the American Academy of Dermatology*, vol. 42, no. 3, pp. 389–416, 2000.

[2] M. Wainwright, "Local treatment of viral disease using photodynamic therapy," *International Journal of Antimicrobial Agents*, vol. 21, no. 6, pp. 510–520, 2003.

[3] A. P. Castano, P. Mroz, and M. R. Hamblin, "Photodynamic therapy and anti-tumour immunity," *Nature Reviews Cancer*, vol. 6, no. 7, pp. 535–545, 2006.

[4] M. Pineiro, M. M. Pereira, A. M. D. Rocha Gonsalves, L. G. Arnaut, and S. J. Formosinho, "Singlet oxygen quantum yields from halogenated chlorins: potential new photodynamic therapy agents," *Journal of Photochemistry and Photobiology A: Chemistry*, vol. 138, no. 2, pp. 147–157, 2001.

[5] W. S. Chan, R. Svensen, D. Phillips, and I. R. Hart, "Cell uptake, distribution and response to aluminium chloro sulphonated phthalocyanine, a potential anti-tumour photosensitizer," *British Journal of Cancer*, vol. 53, no. 2, pp. 255–263, 1986.

[6] J. Moan, Q. Peng, J. F. Evensen, K. Berg, A. Western, and C. Rimington, "Photosensitizing efficiencies, tumor- and cellular uptake of different photosensitizing drugs relevant for photodynamic therapy of cancer," *Photochemistry and Photobiology*, vol. 46, no. 5, pp. 713–721, 1987.

[7] M. C. DeRosa and R. J. Crutchley, "Photosensitized singlet oxygen and its applications," *Coordination Chemistry Reviews*, vol. 233-234, pp. 351–371, 2002.

[8] E. Zenkevich, E. Sagun, V. Knyukshto et al., "Photophysical and photochemical properties of potential porphyrin and chlorin photosensitizers for PDT," *Journal of Photochemistry and Photobiology B Biology*, vol. 33, no. 2, pp. 171–180, 1996.

[9] E. Crescenzi, L. Varriale, M. Iovino, A. Chiaviello, B. M. Veneziani, and G. Palumbo, "Photodynamic therapy with indocyanine green complements and enhances low-dose cisplatin cytotoxicity in MCF-7 breast cancer cells," *Molecular Cancer Therapeutics*, vol. 3, no. 5, pp. 537–544, 2004.

[10] J. M. Fernandez, M. D. Bilgin, and L. I. Grossweiner, "Singlet oxygen generation by photodynamic agents," *Journal of Photochemistry and Photobiology B: Biology*, vol. 37, no. 1-2, pp. 131–140, 1997.

[11] S. Reindl, A. Penzkofer, S. H. Gong et al., "Quantum yield of triplet formation for indocyanine green," *Journal of Photochemistry and Photobiology A Chemistry*, vol. 105, no. 1, pp. 65–68, 1997.

[12] K. Chaudhuri, R. W. Keck, and S. H. Selman, "Morphological changes of tumor microvasculature following hematoporphyrin derivative sensitized photodynamic therapy," *Photochemistry and Photobiology*, vol. 46, no. 5, pp. 823–827, 1987.

[13] L. Ma and D. Dolphin, "Stereoselective synthesis of new chlorophyll a related antioxidants isolated from marine organisms," *Journal of Organic Chemistry*, vol. 61, no. 7, pp. 2501–2510, 1996.

[14] R. K. Pandey, D. A. Bellnier, K. M. Smith, and T. J. Dougherty, "Chlorin and porphyrin derivatives as potential photosensitizers in photodynamic therapy," *Photochemistry and Photobiology*, vol. 53, no. 1, pp. 65–72, 1991.

[15] K. M. Smith, D. A. Goff, and D. J. Simpson, "Meso substitution of chlorophyll derivatives: direct route for transformation of bacteriopheophorbides d into bacteriopheophorbides c," *Journal of the American Chemical Society*, vol. 107, no. 17, pp. 4946–4954, 1985.

[16] K. M. Smith and D. A. Goff, "Synthesis of nickel(II) isobacteriochlorins from nickel(II) complexes of chlorophyll derivatives," *Journal of the American Chemical Society*, vol. 107, no. 17, pp. 4954–4964, 1985.

[17] D. V. O'Connor and D. Phillips, *Time-Correlated Single Photon Counting*, Academic Press, London, UK, 1984.

[18] J. H. Ha, G. Y. Jung, M. S. Kim, Y. H. Lee, K. Shin, and Y. R. Kim, "Efficiency factors of singlet oxygen generation from core-modified expanded porphyrin: tetrathiarubyrin in ethanol," *Bulletin of Korean Chemical Society*, vol. 22, no. 1, pp. 63–67, 2001.

[19] J. H. Ha, S. W. Ko, C. H. Lee, W. Y. Lee, and Y. R. Kim, "Effect of core atom modification on photophysical properties and singlet oxygen generation efficiencies: tetraphenylporphyrin analogues core-modified by oxygen and/or sulfur," *Chemical Physics Letters*, vol. 349, no. 3-4, pp. 271–278, 2001.

[20] A. S. L. Derycke, A. Kamuhabwa, A. Gijsens et al., "Transferrin-conjugated liposome targeting of photosensitizer $AlPcS_4$ to rat bladder carcinoma cells," *Journal of the National Cancer Institute*, vol. 96, no. 21, pp. 1620–1630, 2004.

[21] D. Lim, S. Ko, C. Lee, W. Ahn, and W. Lee, "DH-I-180-3-mediated photodynamic therapy: biodistribution and tumor vascular damage," *Photochemistry and Photobiology*, vol. 82, no. 2, pp. 600–605, 2006.

[22] W. Y. Lee, D. S. Lim, S. H. Ko et al., "Photoactivation of pheophorbide a induces a mitochondrial-mediated apoptosis in Jurkat leukaemia cells," *Journal of Photochemistry and Photobiology B: Biology*, vol. 75, no. 3, pp. 119–126, 2004.

[23] B. W. Henderson, S. M. Waldow, T. S. Mang, W. R. Potter, P. B. Malone, and T. J. Dougherty, "Tumor destruction and kinetics of tumor cell death in two experimental mouse tumors following photodynamic therapy," *Cancer Research*, vol. 45, no. 2, pp. 572–576, 1985.

[24] X. Wang, Y. Koyama, H. Nagae, Y. Wada, S. Sasaki, and H. Tamiaki, "Dependence of photocurrent and conversion efficiency of titania-based solar cell on the Qy absorption and one electron-oxidation potential of pheophorbide sensitizer," *Journal of Physical Chemistry C*, vol. 112, no. 11, pp. 4418–4426, 2008.

[25] J. D. Petke, G. M. Maggiora, L. L. Shipman, and R. E. Christoffersen, "Stereoelectronic properties of photosynthetic and related systems. Ab initio configuration interaction calculations on the ground and lower excited singlet and triplet states of magnesium chlorin and chlorin," *Journal of Molecular Spectroscopy*, vol. 73, no. 2, pp. 311–331, 1978.

[26] I. Eichwurzel, H. Stiel, and B. Röder, "Photophysical studies of the pheophorbide a dimer," *Journal of Photochemistry and Photobiology B Biology*, vol. 54, no. 2-3, pp. 194–200, 2000.

[27] J. R. Lakowicz, *Principles of Fluorescence Spectroscopy*, Springer, Oxford, UK, 2000.

[28] N. Venkatramaiah, N. Veeraiah, and R. Venkatesan, "Spectroscopic and dielectric studies of meso-tetrakis(p-sulfonatophenyl) porphyrin doped hybrid borate glasses," *Journal of Alloys and Compounds*, vol. 509, no. 6, pp. 2797–2803, 2011.

[29] K. Wang, K. Choi, H. Shin et al., "Photophysics of a new photosensitizer with high quantum yield of singlet oxygen generation and its application to stereo-selective synthesis of (+)-deoxoartemisinin," *Chemical Physics Letters*, vol. 482, no. 1–3, pp. 81–86, 2009.

[30] C. Grewer and H. D. Brauer, "Mechanism of the triplet-state quenching by molecular oxygen in solution," *The Journal of Physical Chemistry*, vol. 98, no. 16, pp. 4230–4235, 1994.

[31] C. Gerwer and H. D. Brauer, "Temperature dependence of the oxygen Quenching of $\pi\pi*$-Singlet and $\pi\pi*$-triplet states of singlet oxygen sensitizers," *The Journal of Physical Chemistry*, vol. 97, no. 19, pp. 5001–5006, 1993.

[32] F. Rancan, A. Wiehe, M. Nöbel et al., "Influence of substitutions on asymmetric dihydroxychlorins with regard to intracellular uptake, subcellular localization and photosensitization of Jurkat cells," *Journal of Photochemistry and Photobiology B: Biology*, vol. 78, no. 1, pp. 17–28, 2005.